Title

Novel multi-functional europium-doped gadolinium oxide nanoparticle aerosols facilitate the study of deposition in the developing rat lung

Journal

Nanoscale, 8(22)

ISSN

2040-3364

Authors

Das, Gautom K

Anderson, Donald S

Wallis, Chris D

et al.

Publication Date

2016-06-02

DOI

10.1039/c6nr00897f

Peer reviewed

Published in final edited form as:

Nanoscale. 2016 June 2; 8(22): 11518–11530. doi:10.1039/c6nr00897f.

Novel Multi-functional Europium-Doped Gadolinium Oxide Nanoparticle Aerosols Facilitate the Study of Deposition in the Developing Rat Lung

Gautom K Das[a,*], **Donald S Anderson**[b,*,†], **Chris D Wallis**[a], **Sarah A. Carratt**[b], **Ian M Kennedy**[a], and **Laura S Van Winkle**[b,c,**]

[a]Department of Mechanical and Aerospace Engineering, University of California, Davis, CA, USA 95616

[b]Center for Health and the Environment, University of California, Davis CA, USA 95616

[c]Department of Anatomy, Physiology and Cell Biology, School of Veterinary Medicine, University of California, Davis CA, USA 95616

Abstract

Ambient ultrafine particulate matter (UPM), less than 100 nm in size, has been linked to the development and exacerbation of pulmonary diseases. Age differences in susceptibility to UPM may be due to a difference in delivered dose as well as age-dependent differences in lung biology and clearance. In this study, we developed and characterized aerosol exposures to novel metal oxide nanoparticles containing lanthanides to study particle deposition in the developing postnatal rat lung. Neonatal, juvenile and adult rats (1, 3 and 12 weeks old) were nose only exposed to 380 $\mu g/m^3$ of ~30 nm europium doped gadolinium oxide nanoparticles (Gd_2O_3:Eu^{3+}) for 1 h. The deposited dose in the nose, extrapulmonary airways and lungs was determined using inductively-coupled plasma mass spectroscopy. The dose of deposited particles was significantly greater in the juvenile rats at 2.22 ng/g body weight compared to 1.47 ng/g and 0.097 ng/g for the adult and neonate rats, respectively. Toxicity was investigated in bronchoalveolar lavage fluid (BALF) by quantifying recovered cell types, and measuring lactate dehydrogenase activity and total protein. The toxicity data suggests that the lanthanide particles were not acutely toxic or inflammatory with no increase in neutrophils or lactate dehydrogenase activity at any age. Juvenile and adult rats had the same mass of deposited NPs per gram of lung tissue, while neonatal rats had significantly less NPs deposited per gram of lung tissue. The current study demonstrates the utility of novel lanthanide-based nanoparticles to study inhaled particle deposition *in vivo* and has important implications for nanoparticles delivery to the developing lung either as therapies or as a portion of particulate matter air pollution.

Graphical Abstract

**Corresponding Author: lsvanwinkle@ucdavis.edu.
*GKD and DSA contributed Equally to this work
†Present Address: Center for Environmental Health Sciences, University of Montana, Missoula MT, USA 59812.

Electronic Supplementary Information (ESI) available: [details of any supplementary information available should be included here]. See DOI: 10.1039/x0xx00000x

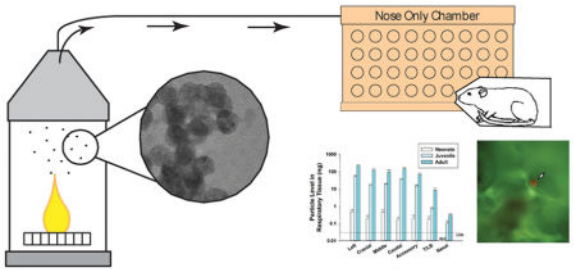

Introduction

Humans inhale thousands of liters of air, containing potentially billions of particles each day, but only a fraction of these particles deposit on the lung surface.[1] It is a basic tenet of toxicology that the biologic response is proportional to the local dose but the study of the inhalation toxicology of small particles is hampered by the inability to measure the delivered, local, dose for nanoparticles in a precise, cost effective, and scalable manner. Complicating this is that ultra-fine and nano-sized materials are very difficult to observe in the large surface area and complex cellular environment of the lung.

Previous studies have employed many different tracer particles to study particle deposition and biodistribution. Ideally, a tracer particle should be easy to aerosolize, scalable to large exposure studies, as well as readily quantifiable with superior sensitivity. Most importantly, the tracer particle should be stable, nontoxic and, preferably, optically active, thus allowing its movement and interactions with cells to be tracked over time. Though some tracer particles are in limited use, widespread use of tracer particles has not been possible to date due to high cost, difficulty in aerosolization or concerns over cytotoxicity. Currently used tracers include fluorescently labeled particles such as polystyrene beads[2] or quantum dots.[3] Radioactive particles or particles with radioactive tags have also been used to study deposition and translocation.[4, 5] However, there are significant limitations to these methods. First, the wet-chemical synthesis of fluorescent nanoparticles is not representative of environmentally relevant particles. The likelihood of these types of particles being inhaled in aerosolized form is extremely low and so they do not represent a realistic environmental exposure scenario. Second, most current particle fluorescence detection methods are not sufficiently sensitive to monitor low levels of particles. Further, particle fluorescence is susceptible to alteration due to the local physiological conditions resulting in loss or separation of the signal from the particle. Additionally, the use of aerosolized radioactive particles requires specialized facilities to prevent the accidental release of these materials. Finally, radioactive tags also have limitations due to detachment of the tag or dissolution of the particle. Therefore, an ideal tracer particle should resemble environmentally or occupationally relevant nanoparticles and encompass the relevant surface properties. One class of environmentally similar nanoparticles with many industrial uses is flame-generated metal and metal oxide nanoparticles. Flame based synthesis of nanoparticles is one of the preferred routes used in industry, and this method accounts for the highest volume of nanomaterial production.[6, 7] Further, the protein adsorption layer on the surface of flame-

generated metal oxide particles closely mimics, fugitive dust PM [8, 9] as well as a number of well-studied aerosolized nanomaterials.[10]

Cost effective scalable tracers are critically needed in toxicology where species, strain, age, nasal and respiratory tract anatomic differences, disease, physiology and history of prior exposure can all result in altered deposition to the respiratory tract, changing both total and local delivered dose. While the impact of physiologic parameters on particle deposition in relation to respiratory air flow patterns has been investigated[11–13], little is known about the fate of inhaled nanoparticles,[14] some of which are found in ambient air, in occupational settings or as part of inhaled therapeutics. Data are especially scarce for the developing lung or the effect of lung disease on deposition of particles in the nanosize range. Data on particle deposition in the developing lung is important because children are uniquely susceptible to inhaled PM; studies show that children living in close proximity to PM sources have a greater incidence of respiratory diseases.[15] Furthermore, many studies have shown that the developing lung is not the same as an adult lung; the developing lung responds to inhaled compounds differently, sometimes with enhanced cytotoxicity and inflammation.[16–18]

Recently, we reported the use of flame-generated luminescent gadolinium oxides to study translocation and clearance of intratracheally instilled particles.[8] Luminescent lanthanide nanomaterials have been widely investigated for biomedical applications due to their unique optical properties.[19–23] Here, we use lanthanides as a powerful tracer to detect deposition following aerosol inhalation at extremely low concentrations by taking advantage of the very low natural abundance of lanthanides in the body. Detection of lanthanide tracer particles via inductively coupled plasma mass spectroscopy (ICP-MS) can trace low levels, on the order of parts per trillion, with almost no background signal. We have developed a unique aerosol with an environmentally relevant lanthanide-containing metal oxide that was generated using a flame system (Figure 1). The flame system permits on-line exposure to freshly generated nanoparticles. The particle exposure system is significantly different from common aerosol generators used to disperse nanopowders such as nebulizers, fluidized beds and venturi-type systems. The ease of generation and the extremely high detection sensitivity make flame synthesized lanthanide oxide nanoparticles an excellent choice for the study of deposition, translocation and toxicity following exposure to a particulate aerosol.

In the current study, we show that an extremely low level of deposited inhaled nanoparticles is conveniently detectable using flame synthesized Gd_2O_3:Eu^{3+} nanoparticles in rats. Gd_2O_3 was chosen because it constitutes a good host matrix for luminescent lanthanides ions. In addition, gadolinium shows paramagnetism which makes Gd_2O_3 a very attractive choice to dope with different lanthanide ions for achieving bifunctionality (i.e. paramagnetism and bright emission). The rat model was used to study age differences in particle deposition because rats, similar to humans, are born with lungs at the saccular stage and go through the same alveolar remodeling processes postnatally.[24] The experimentally obtained dose was then compared with two commonly used computational models of theoretical particle deposition: the International Commission on Radiological Protection model (ICRP)[25] and the Multipath Particle Dosimetry model (MPPD).[26] Toxicity of the nanoparticles was also investigated. Here we demonstrate that 1) extremely sensitive detection is possible in animals with different levels of expected deposition 2) the particles can be localized in the

lung tissue and 3) $Gd_2O_3:Eu^{3+}$ particles are not acutely toxic even at high dose (380 μg/m^3). Thus $Gd_2O_3:Eu^{3+}$ NPs are an optimal tracer particle for the study of nanoparticle deposition, clearance and cellular interactions following a relevant inhalation exposure.

Results

Particle Characterization

Figure 2a shows a TEM image of the synthesized $Gd_2O_3:Eu^{3+}$ NPs electrostatically precipitated onto a TEM grid. The morphology is spherical and the size distribution suggests an average size of 29 ± 7 nm (n > 100). The mobility diameter distribution of the nanoparticles obtained from scanning mobility particle sizer (SMPS) shows a geometric mean size of 31.1 nm (Figure 2b) which is in good agreement with the observed TEM size. In this system, particle size can be tuned by changing the concentration of the precursor and spray droplet size during pyrolysis. However, we chose to perform our experiment with particles of ~31 nm as particles of similar size range (>30 nm) have previously been shown to lack rapid clearance from lung.[3] The crystallinity of the nanoparticles was analyzed by powder X-ray diffraction - the XRD pattern (Figure S1a) of the synthesized NPs is matched well with the cubic Gd_2O_3 (JCPDS #12-0797).[27] The specific surface area of the NPs was obtained from the nitrogen adsorption/BET method and estimated as 21.12 m^2/g (Figure S1b).

The photoluminescence (PL) spectrum of the synthesized NPs dispersed in the milliQ water is presented in Figure 3A showing three characteristic emission peaks at 590, 613, and 623 nm which correspond to $^5D_0 \rightarrow {}^7F_1$, $^5D_0 \rightarrow {}^7F_2$, and $^5D_0 \rightarrow {}^7F_3$ transitions respectively.[28] The dominant peaks at 613 and 623 nm emit red as shown in the photograph (Figure S2). The excitation spectra of the $Gd_2O_3:Eu^{3+}$ nanoparticle suggests that the strongest band is centered at ~255 nm while other bands appear at 326, 361, 378, 393, 432, 465, and 535 nm.[29] Therefore, a wavelength of 254 nm (a conveniently available Xenon lamp) was used for excitation for the purpose of optical characterization. This wavelength was not available on the fluorescence microscope. Hence, a wavelength of 340–380 nm was used for the imaging studies. A comparison in the PL spectra at two excitation sources is presented in Figure S3.

Photoluminescence provides an ideal indicator of dissolution kinetics (if any) of the NPs and enables us to determine whether the particles dissolve at different pH or in physiological conditions such as in the lung fluid. In our previous work, we showed that the flame synthesized $Gd_2O_3:Eu^{3+}$ NPs are very stable between pH 4 to 7.[8] Here, we found similar stability for our synthesized NPs in phosphate buffered saline (PBS) and in lung lavage fluid. As shown in Figure 3B the integrated PL intensities (determined by area under the curve) of the NPs were very steady over time, which implies that there is no discernable dissolution of the NPs ; the dopant (Eu^{3+}) ions remain well-protected in the host crystal matrix (i.e. Gd_2O_3).

Exposure Characterization

Exposure conditions are summarized in Table 1. The geometric mean particle diameter was 31.1 nm σ_g 1.6, indicating a polydispersed distribution of the nanoparticles. The exposure mean mass concentration was 380 μg/m^3 and the mean particle number concentration 7.4×10^5 cm^{-3}, The particle concentration was reasonably stable for the duration of the three exposures as demonstrated in Figure S4. The presence of possibly toxic gasses was measured and found to be at acceptable levels. Carbon monoxide (CO) was below the level of quantification for the instrument, less than 0.5 ppm. Nitric oxide (NO) and nitrogen dioxide (NO_2) were both at 0.45 ppm when undiluted burner output was measured. Testing for volatile organic compounds (VOC) on undiluted burner output was 0.2 ppm. Since the burner output stream is diluted 10:1 with dried and filtered air, a much lower level in the exposure chamber, within allowable limits for biological exposures, was expected. Dilution flow conditions were set to ensure that the chamber temperature never exceeded 1°C above the ambient room temperature. In testing, the normal chamber humidity was 6% due to the use of dried dilution air. To provide a reasonable exposure humidity, dilution air containing more water vapor was used for a target humidity level of 30 to 35%.

Deposition

Male Sprague-Dawley rats, 1 week (neonate), 3 weeks (juvenile) and 8 weeks (adult), were exposed in a nose-only exposure system for 1 h to an average particle concentration of 380 μg/m^3. The mass of Gd_2O_3:Eu^{3+} NPs deposited in the respiratory system was measured in the extrapulmonary airways (trachea and primary bronchi), in the nasal epithelium and in each lung lobe separately using ICP-MS of digested tissue. These data show that the adult rats had the greatest mass of NPs deposited in all respiratory tract regions (Figure 4a). However, this does not take into account the difference in animal size by age. When deposited mass was normalized by the dry weight of the tissue, adult and juvenile rats had a similar deposited mass, with the exception of the extra-pulmonary airways (Figure 4b). However, neonatal rats had a deposited mass of nanoparticles per gram of tissue, significantly less than juvenile and adult rats. Juvenile rats received a dose that was 40% greater than adult rats when exposed to the same atmosphere. The nasal deposition of nanoparticles was assessed by measuring Eu and Gd in the nasal epithelial tissues (Figure 4). The mass of Eu and Gd measured in the nose was much lower than that deposited in the lung. Nasal doses in neonatal animals were below the limit of detection, while juvenile and adult rats had nanoparticle levels below 10 ng/g dry tissue weight. The lung deposition in both juveniles and adults exceeded 1000 ng/g. Pulmonary deposition is 100 times greater than nasal deposition when normalized for tissue mass. When delivered dose was calculated, yielding the total mass of particles for a given body weight, the juveniles received a significantly greater dose than either adult or neonatal rats (Figure 5a). The adult dose was also significantly greater that that received by the neonatal rats. When particle deposition was compared to the size of the lung, determined by tissue mass, both juvenile and adult rats had significantly greater lung dose than neonates (Figure 5b). While there was a trend toward greater deposition in the adult rat lung compared to the juveniles, when comparing dose per mass of lung tissue, this increase was not statistically different.

Toxicology

To assess acute toxicity or inflammation due to exposure to our aerosol materials, the following indicators of response were measured in all three age groups: total cells in BALF; BALF cell differentials; and BALF levels of protein and lactate dehydrogenase activity as a measure of LDH levels 24 h after exposure (Figure 6). There was no significant difference between control and particle-exposed animals for total cells in BALF (Figure 6a). There was an age dependent difference in total cells recovered; this could be attributed to the volume of lavage fluid used for different size animals. BALF cell differentials indicate no acute inflammatory response to nanoparticle exposure. In all groups, macrophages made up 98 to 99% of the recovered BALF leukocytes (Figure 6b). There was a significant increase in BALF protein in the exposed neonates (Figure 6c). LDH in BALF, an indicator of cellular damage, was not significantly different from control animals for each of the age groups (Figure 6d). The lack of increase in BALF LDH levels indicates that the NPs are generally not toxic; however, the increase in protein in BALF in neonatal rats could be caused by increased capillary permeability in that age group.

Imaging

The strongest emission peak of Gd_2O_3:Eu^{3+} NPs appears at 610–620 nm. Figure 7 demonstrates the ability to visualize these NPs in the tissue with a fluorescent microscope (excitation using a mercury metal halide lamp and UV transmission filter). At 24 h post exposure, an alveolar macrophage (arrow) can be seen with an accumulation of internalized Gd_2O_3:Eu^{3+} NPs. Enhanced dark field microscopy (Figure 8a) shows deposition of Gd_2O_3:Eu^{3+} NPs on the epithelium in the gas exchange region of the lung in an adult rat. Figure 8b shows the spectral profile of the deposited Gd_2O_3:Eu^{3+} NPs using hyperspectral imaging. Image pixels of deposited particles are identified by the unique spectrum generated by the particles between 450 nm and 850 nm (red and green lines) compared to tissue without particles (yellow line). A control spectrum for the Gd_2O_3:Eu^{3+} NPs was generated from a particle only sample (data not shown) and compared pixel-by-pixel to spectral data from tissue samples to identify regions of particle deposition. H&E stained tissue sections (Figure 9) illustrate the developmental difference between animals at the different ages used in this study. Neonatal rats have yet to complete alveolar development (Figure 9a), juvenile rats possess small, but fully developed alveoli (Figure 9b) and adults have enlarged mature alveoli (Figure 9c). Lung tissue was examined for indications of inflammation including accumulations of leukocytes and none were observed (data not shown).

Modeling

Since models for deposition of particles are limited to adult animals, these methods were not applied to the neonatal and juvenile data. The ICRP model employs published total lung deposition data from both human and several animal models to determine deposition fractions of particles of different sizes.[25] Using the formula: D = MCTF, where D is deposited dose, M is minute volume, C is exposure concentration, T is exposure duration and F is the deposition fraction. The measured concentration of 380 μg/m^3 and published values for minute volume of 214 ml/min, and a pulmonary deposition factor of 0.14,[30] over a 60 min exposure 683 ng of particles would be deposited. The MPPD model is a computer

model that calculates total respiratory system deposition of particles in human and rat models, but also estimates the airway level deposition of inhaled particles.[26] We used the MPPD model to estimate total deposition of particles in rats under the exposure conditions used in this study. Input values and model results are shown in Table 2. In summary, MPPD predicted a pulmonary deposition of 1228 ng. This can be compared to the average measured pulmonary-deposited dose in the adult rats of 648 ng.

Discussion

We used flame pyrolysis to generate lanthanide based metal oxide nanoparticles (Gd_2O_3:Eu^{3+} NPs). We have used this type of nanoparticle previously to demonstrate it's potential as a sensitive method for studying translocation of particles from the lung in mice,[8] but had not used these particles in an inhalation exposure system where deposition will be a major factor in determining local dose. In this current study, we established that these particles can be used for aerosol exposures. To test the utility of the system, we exposed rats at three different ages to a well-characterized aerosol of the Gd_2O_3:Eu^{3+} NPs. We chose these ages because particle deposition is known to differ between them and indeed we did find significant differences in delivered dose by age, proving the utility of these particles to detect known differences in deposition. Using the known ratio of Gd:Eu, our data also indicate that the Gd_2O_3:Eu^{3+} NPs remain intact and that their native fluorescence can be used to image them within cells in the lung. We also found that, of the two models used to predict the deposition of particles in adult rats, the ICRP based mathematical calculation (683 ng) was closer to our experimental data (684 ng) than the MPPD computer model (1228 ng). Finally, we demonstrated that the nanoparticles generated for this study did not cause overt acute lung toxicity or inflammatory cell recruitment.

We assessed deposition by measuring mass of nanoparticles deposited in each of the lung lobes, the trachea/extra-pulmonary bronchi and the nasal epithelium using ICP-MS (Figure 4a). The deposited mass of nanoparticles was significant between all ages with adult > juvenile > neonate (Table S1a). This result is expected given the size difference, and therefore larger lung volume and respiratory volumes, of the different age animals. However, total particle deposition should be looked at in terms of relative burden for the age of the animals. Therefore, we examined the deposition of Gd_2O_3:Eu^{3+} NPs as a dose per lung size, as determined by tissue mass, and animal body weight. The deposited mass of nanoparticles in relation to lung size, did not differ between the juvenile and adult rats. Further, the dose of particles by body weight shows that the juvenile rats received a significantly greater dose than either the neonates or adults. This is in agreement with other work that shows that the deposition fraction of nano-sized particles in 7-day-old rats is very low, peaks at 21 day of age and then declines in adulthood.[11] Structural differences in the gas exchange region of the lung in different age rats (Figure 9) is likely a major contributing factor. Other studies have reported that air mixing, and therefore nanoparticle deposition, is affected by alveolar size and shape. [12, 13] Our results are in agreement of this explanation of age differences in nanoparticle deposition.

In addition to total deposition, we measured deposition in the lung lobes of the rats (Figure 4). While differences in mass of nanoparticles between different lobes was observed, when

the deposited dose was normalized for the size of the lobe, as defined by the dry weight, there was little lobe-to-lobe difference in deposition. In fact, the only significant differences seen in lobes of same age animals were between adult cranial and caudal lobes ($p = 0.029$) and neonate middle and accessory lobes ($p = 0.022$). Studies of lobe-to-lobe distribution patterns of nanoparticles in laboratory animals are lacking as most studies of distribution have focused on central versus peripheral distribution in the lung (by airway generation) and typically used particles larger than 100 nm.[31, 32] One study performed in Wistar rats using 1.2 μm iron oxide particles did find a statistical difference in particle deposition between the cranial and accessory lobes of healthy animals.[33] Studies in human subjects have shown left/right lobe differences in particle deposition that is effected by breathing pattern and disease state.[34, 35] Therefore, it is reasonable to observe difference in lung lobe-to-lobe distribution of particles.

Because rats are obligate nose breathers, deposition was measured in the nose. There were very low levels of deposition in all age groups, with the neonatal deposition below the level of detection. This may be due to the size of the particle; 30 nm particles have been previously reported to be ineffectively deposited in the nose.[36] We sampled the entire nasal epithelium for all age groups. In doing so, we recognize that we did not account for localized deposition in different nose regions, which could be a focus of future studies using these particles. Garcia et al. used computational fluid dynamics to predict that nearly 70% of 30 nm particles deposited in the respiratory and olfactory epithelium of the nose.[37] Additionally, it has been reported that rats younger than 11 days old have undefined turbinates in the nose and this may also have contributed to the lack of detectable deposition in this age group and may change deposition by age in focal regions of the nose.[38]

Dose is related to body size, which was increasing with age in this study. Therefore, we calculated delivered dose normalized to body weight so that the results of this study can be compared to studies where doses are directly administered to the lung by intratracheal administration. The juvenile rats had a significantly higher dose than either the neonatal or the adult rats (Figure 5). A previous study observed a similar pattern in rats ages 7, 14, 21, 35 and 90 days of age following exposure to 20 and 80 nm-radiolabeled nanoparticles, with 21 day rats having the greatest deposited fraction.[11] To understand this result, one must consider the structure of the gas exchange region of the lung and how it changes in the postnatal period. Neonatal rats have undeveloped acini, but undergo exponential growth in the first 21 days.[39–41] At this point, the number of alveoli are set and only grow in size. This is illustrated with the animals used in this study in Figure 9. A major contributor to increased deposition in the juvenile rats is likely the large number of smaller alveoli at that age due to normal septation followed by growth. Nano-sized particle deposition in the deep lung is driven by Brownian diffusion, while gravity and particle density are insignificant factors.[13] Therefore, the distance a particle needs to travel to deposit on tissue will be an important element in deposition. We were able to use these exposure experiments to gauge the effect of animal age on the deposited dose of inhaled nanoparticles. Juvenile rats received the largest dose due to their fully developed but small alveoli, in agreement with previously published studies on the effects of alveolar development on nanoparticle deposition.[42]

The comparison of experimental data and models of deposition is important for validating the models. In this study, a measured deposition was compared to calculated deposition using both a simple mathematical calculation (ICRP) and to a software model (MPPD). There is reasonable agreement between the predicted dose and the results of this study, with the ICRP model predicting a 5.6% greater dose, 683 ng versus 648 ng. The deposition fraction of 0.14 is based on a larger particle, 290 nm and in the Fischer 344 rat.[30] The MPPD model software predicted two fold more nanoparticle deposition than what we measured in the lung. Due to the limited data on particles that are less than 100 nm, the MPPD model uses theoretical predictions of particle deposition from diffusion and uses the lung geometry of the Long-Evans rat.[43] Resent work has shown that the deposition fraction for nanoparticles between 10 nm and 100 nm could be a significantly lower in Sprague-Dawley rats than in the Long-Evans rats and this may be the source of the departure from what we measured.[44] Unlike simple dose calculations, the MPPD model provides regional deposition factions that could be useful in the study of specific lung regions and future studies using these particles could serve to analyze the accuracy of these predictions. Our results suggest that using the MPPD with rat stains other than the Long-Evans rat should be done with care. An increased body of experimental data would facilitate the improvement in these models, allowing more accurate extrapolation to human exposure levels from animal toxicology studies.[45]

An acute exposure to Gd_2O_3:Eu^{3+} NPs did not produce overt toxicity or acute inflammatory responses in adult and juvenile rats, and the only toxicity-associated parameter that was increased was BALF protein in neonates. This indicates that the exposure to Gd_2O_3:Eu^{3+} NPs may increase capillary leakage of serum proteins into the lung gas-exchange region of neonate rats. Compared to other particles we have tested in 7 day old rats, the amount of the protein in lavage fluid is quite low. Protein and LDH in BALF are common measures of toxicity in the lung and it is notable that there was no difference in LDH activity by age, indicating a lack of frank cytotoxicity from the particle exposure. Based on our current deposition results for nanoparticles, it is unlikely that the neonates were more susceptible due to an increased dose delivered. Thus, we conclude that there may be an intrinsic response of the developing lung to nanoparticles that results in increased protein in the BALF. This may be due to differences in the local alveolar cell interactions with particles at this very young age resulting in more protein leak. This is in contrast with a previous study of high PAH containing flame generated soot of similar size (70 nm) where both adult and 7 day old rats received a single acute inhalation exposure.[46] The exposure dose in this other study was less than half of our current study, yet the soot particle exposure produced a significant increase in neonatal BALF LDH activity 24 hours post exposure, with neonates more susceptible than adults.[46] This again supports that there may be an intrinsic difference between neonatal and adult lungs in respect to particle interactions.

At 24 h post-exposure, we examined the BALF cell population and found no statistical difference in cell types or number of cells recovered indicating that there was not an acute inflammatory response to the nanoparticle exposure. Macrophages are the predominant inflammatory cell type resident in the lung, often comprising 98% or more of the cells recovered in BALF. Acute exposures to ultrafine PM frequently involve recruitment of neutrophils.[46] Neither macrophages nor neutrophils increased in the BALF of exposed

animals at 24 h. Typically, 24 h are long enough after exposure to see any particle associated BALF cellular infiltrates. Histology of the lung tissue also did not find tissue damage or inflammation at any age. This coupled with no histologic evidence of inflammation or BALF cell changes, leads us to conclude that these particles lack overt toxicity.

We demonstrated three microscopy methods of identifying the Gd_2O_3:Eu^{3+} NPs in tissue lung tissue samples. Using fluorescence microscopy, we could image agglomerates of particles. This can occur after a phagocytic cell takes up a large number of the particles as demonstrated in Figure 7. The resolving power of fluorescence microscopy precludes imaging of the individual particles, which are approximately 30 nm. Enhanced darkfield imaging (Figure 8a) captures the scatted light from the Gd_2O_3:Eu^{3+} NPs. Since the particles are not directly imaged, but rather their scattered light, this method can identify particles in the nano-size range. What we see is a wide distribution of particles deposited in the gas exchange region of the lung. Hyperspectral imaging (Figure 8b), when used with enhanced darkfield microscopy, confirms that the scattered light seen in the enhanced darkfield image is caused by the Gd_2O_3:Eu^{3+} particles. Figure 8a shows a full range of emission spectra for the Gd_2O_3:Eu^{3+} nanoparticle that indicate its characteristic emission peaks at ~580, ~600, ~620, ~ 680 and ~700 nm. We observed a slight red shift in the spectra compare to the nanoparticles dispersed in milli-Q water (Figure 3a). A small red shift is a fairly common phenomena for Eu-doped phosphor where a number of factors contribute to the shift including type of solution, crystal field, excitation wavelength and type of excitation sources.[29, 47] In our case, we believe media of the nanoparticle, and different excitation source may attribute to the shift.

Conclusions

We developed a system capable of generating an atmosphere of occupationally and environmentally relevant metal oxide nanoparticles. We performed extensive testing to confirm that there were no gas phase combustion by-products that could induce toxicity in the atmosphere as CO, NO, NO_2, and VOCs were monitored and were within normal ranges. Exposure of 3 ages of rats determined that this exposure method is sufficiently sensitive and robust to detect differences in deposition of NPs by age. We were able to compare measured deposition to common methods of calculating particle deposition. The NPs generated were not acutely cytotoxic or inflammatory in the lung, which will be important for future studies of NP trafficking in cells and tissues. In conclusion, this method is capable of assessing the deposition and fate of nanoparticles deposited in the lung.

This study demonstrates the utility of flame generated lanthanide based nanoparticles for studying particle deposition in the developing lung. Future research could use this approach to study particle translocation and clearance, the effect of pre-existing diseases on particle deposition and clearance, as well as the interaction of specific cell types with these particles. A key finding from this study is that neonatal rats do not receive a greater delivered dose than adult rats. In fact, juvenile rats received the greatest dose following a nose only inhalation exposure, indicating that this intermediate point in lung development could result in the greatest biological effect from airborne particles. Information about delivered dose is

key to interpretation of toxicological studies of ultrafine particulate matter as well as extremely important to design nanoparticle mediated pulmonary drug delivery systems.

Methods

Chemicals

All chemicals were analytical grade or better. The $Gd(NO_3)_3.6H_2O$, and $Eu(NO_3)_3.6H_2O$ were purchased from Sigma Aldrich. Compressed hydrogen and nitrogen gas was supplied from Praxair Inc. (San Ramon, CA) with stated purity of 99.5% or higher. Milli-Q ultrapure (>18.3 MΩ-cm) water was used to generate precursor solution and dilute ICP-MS samples. The 70% trace metal grade nitric acid was purchased from Fisher Scientific and 30% hydrogen peroxide was purchased from EMD Millipore.

Inhalation Exposure System Design and Operation

Figure 1 illustrates our particle synthesis and exposure system. The system is capable of generating environmentally relevant $Gd_2O_3:Eu^{3+}$ NPs and can be used for either nose-only or whole body animal exposures. The aerosolized $Gd_2O_3:Eu^{3+}$ NPs were synthesized using a flame pyrolysis reactor.[8, 48] Aerosol from this reactor was cooled, dehumidified and diluted into an exposure chamber for inhalation studies (see inhalation exposure system description below). The liquid precursor was prepared by dissolving 2 mmol of $Gd(NO_3)_3.6H_2O$ and 0.45 mmol of $Eu(NO_3)_3.6H_2O$ in 500 ml of MΩ water. The precursor solution was fed to an ultrasonic spray nozzle (Sono-Tek Corporation, Milton, NY) in the burner at 30 ml/h using a single syringe infusion pump (Cole-Parmer, Vernon Hills, IL). The ultrasonic spray nozzle (Sono-Tec, Milton, NY) maintained a high precursor loading while narrowing the droplet size distribution. The N_2 flow carried the precursor droplets into the H_2 generated flame. The liquid droplets were thermally decomposed in the hydrogen-air flame to form the desired NPs.

The exposure system operated by drawing HEPA filtered room air at 24 l/min into the bottom of an aluminium and glass housing containing the flame pyrolysis reactor (burner). Output from the burner was drawn out the top of the housing through stainless steel pipe. The aerosol stream was cooled and the flow was split with excess NPs collected in a filter connected to a high volume vacuum pump. Water from the combustion of H_2 was removed from the particle stream using a diffusion dryer (TSI Inc., Shoreview, MN). The continuously generated aerosol was diluted at a ratio of 1:10 with filtered dry air before entering the nose-only exposure chamber.[49] A typical flow rate of 15 l/min was maintained through the chamber. The chamber was held at slightly negative pressure (−0.5 inches H_2O relative to ambient) to prevent particle release from the system. Pressure was monitored continuously with a Magnehelic® differential pressure gauge (Model 2002, Dwyer Instruments, Michigan City, IN). Temperature and relativity humidity (RH) were monitored at the location of animal exposure in the chamber using an Amprobe THWD-5 probe humidity and temperature meter (Danaher Corp., Everett, WA).

The CO level during exposure was monitored using a Gas Filter Correlation CO Analyzer (Teledyne API model M300E, San Diego, CA). NO and NO_2 were measured using a

Chemiluminescence NOx Analyzer (Dasibi Corporation model 2108). Volatile organic compounds (VOC) were monitored using a miniRAE 3000 VOC meter (RAE Systems, San Jose, CA). The real-time number concentration of the particles (as a function of size in the exposure chamber) was monitored continuously using a Scanning Mobility Particle Sizer (SMPS) (TSI 3071 classifier and TSI 3010 condensation particle counter, TSI Inc.). Aerosols were sampled from the exposure chamber for gravimetric analysis at a 5 l/min flow. Particles were collected on pre-weighed 25 mm Pallflex membrane filters (Pall Life Sciences, Port Washington, NY) which were housed in a closed-faced filter cassette. The filters were pre- and post-weighed in a high precision microbalance to determine mass (model XP26, Miller Toledo, Columbus, OH). The filters were also desiccated and re-measured. There was no significant difference between the filter measurements, indicating that moisture did not influence filter mass. Two filter measurements were taken for each exposure.

Animals

Male Sprague-Dawley rats were obtained from Harlan Laboratories (Hayward, CA). Rats were exposed at 1 (neonate), 3 (juvenile) and 12 (adult) weeks of age using a nose only exposure system. All animal experiments were performed under protocols approved by the University of California Davis IACUC in accordance with National Institutes of Health guidelines. Rats of 1 and 3 weeks of age exposures were obtained at 1 day of age and housed with a lactating dam, with 10 pups per dam until use. Adult rats were obtained one week prior to exposure and housed 2 per cage. Rats were subjected to a single acute 1 h nose only exposure to europium doped gadolinium oxide nanoparticles (Gd_2O_3:Eu^{3+} NPs). Control animals were exposed in tubes for 1 hour to the exposure system operating without precursor solution being fed to the burner. Each age and timepoint group had five animals.

Particle Characterization

Morphological characterization of the NPs was determined using a Phillips CM-12 transmission electron microscope (TEM) operated at 120 kV. NPs were suspended in MQ water and deposited on a 400 mesh copper TEM grid with a carbon/Formvar® film (Ted Pella Inc. Redding CA. Prod # 01754-F). The particle crystalline phase was identified using a Scintag powder x-ray diffractometer (XRD) with Cu Kα radiation operated at 45 kV and 40 mA. The PL spectra of particle suspensions were obtained using a Varian Cary Eclipse Fluorescence Spectrophotometer equipped with a Xenon lamp as an excitation source. The surface area of nanoparticles was measured with the Brunauer-Emmett-Teller (BET) method using an Autosorb-1 instrument (Quantachrome Instruments, Boynton Beach, FL). NPs were degassed for 24 h at 150 °C before the measurement. Hydrodynamic particle size measurements were performed using a BIC 90Plus dynamic light scattering instrument (Brookhaven Instruments, Holtsville, NY). Zeta potential was measured by light scattering using a BIC ZetaPlus instrument (Brookhaven Instruments Corporation, NY). At least five measurements were made for each sample and the data were averaged.

Deposition Analysis by ICP-MS

The concentrations of Gd_2O_3:Eu^{3+} NPs in the nose, extra-pulmonary airways and lung lobes were determined using ICP-MS.[8] Immediately after the 1 h exposure, rats were euthanized

with an intraperitoneal injection of pentobarbital (150 mg/kg) and subsequently exsanguinated prior to lung removal. Lungs were removed en bloc from the thoracic cavity and separated by lobe and extra-pulmonary airways, flash frozen and stored at −80°C until processed. The nasal epithelium was removed and flash frozen and stored at −80°C until processed. Tissues were lyophilized using a Labconco FreeZone 2.5 (Kansas City, MO) freeze-drying system and weighed to determine tissue dry weight. Tissue was digested with 70% trace metal grade nitric acid, volume dependent on tissue mass, and heated to 70°C for a minimum of two hours. Samples were cooled to room temperature, and an equal volume of 30% H_2O_2 was added. Samples were then heated to 70°C for 12 hours to break down remaining lipids. After 12 hours, samples were cooled to room temperature and diluted 10:1 with milliQ water for analysis by the UC Davis/Interdisciplinary Center for Plasma Mass Spectrometry using an Agilent 7500CE ICP-MS (Agilent Technologies, Palo Alto, CA). The samples were introduced using a MicroMist Nebulizer (Glass Expansion, Pocasset, MA) into a temperature controlled spray chamber with Helium as the collision cell gas. The ICP-MS instrument was calibrated using a NIST traceable standard for Eu and Gd. The standards came in stock solution at 10003ppb and 1003ppb; serial dilutions of 300, 200 and 1003ppb were used at the high end of the concentration range and 50, 10, 1, 0.5 and 0.253ppb for the low concentration standard to generate the calibration curve.

Lung Tissue Fixation and Histologic Imaging

Animals used for imaging were euthanized at 24 h post exposure as described above. The trachea was cannulated, thorax opened and lung removed en bloc for inflation with 37% formaldehyde vapor bubbled under 30 cm hydrostatic pressure for 1 hour as previously described.[16, 50, 51] Samples were stored in 1% paraformaldehyde for no more than 24 hours prior to tissue processing and paraffin embedment. Paraffin blocks were sectioned at 4 μm onto poly-L-lysine coated slides, H&E stained and imaged with an Olympus BH2 microscope. Whole mount tissues for in situ localization of Gd_2O_3:Eu^{3+} NPs were prepared from the right middle lobe. The lobe was dissected to expose the airways from the interlobar bronchus to terminal bronchioles and surrounding parenchyma region,[52] and imaged using a Leica TCS LSI microscope in fluorescent mode using the metal halide light source, a 340–380 nm band-pass excitation filter, 425 nm emission filter and a 40× water dipping objective.

Spectral profiling and enhanced dark field imaging

Gd_2O_3:Eu^{3+} NPs deposition was qualitatively evaluated in unstained paraffin embedded lung sections using a Cytoviva enhanced dark field microscope (Cytoviva, Auburn, AL). Lung sections were evaluated for qualitative assessment of Gd_2O_3:Eu^{3+} NPs deposition at a magnification of 100x. Spectral analysis of Gd_2O_3:Eu^{3+} NPs was performed utilizing hyperspectral dark field microscopy (Cytoviva, Auburn, AL). To generate a mean spectral profile of Gd_2O_3:Eu^{3+} NPs, particles were loaded onto premium clean microscope slides and mean spectrums were created utilizing pixels with an intensity greater than 1000. Gd_2O_3:Eu^{3+} NPs associated with cells were assessed by focusing on the nucleus of the cell and a hyperspectral image was collected at a magnification of 100x. To generate spectral profiles a minimum of 1,000 pixels of Gd_2O_3:Eu^{3+} NPs were collected to form a region of interest that was used to create a mean spectrum. This spectrum was then normalized and compared to the normalized original spectrum of the corresponding Gd_2O_3:Eu^{3+} NPs.

Bronchoalveolar Lavage Fluid (BALF)

Animals used for the collection of BALF were euthanized 24 h post exposure by the same method as above. Following euthanasia, the trachea was cannulated, the abdomen and thoracic cavity opened, the lung lavaged with 0.9% sterile saline. BALF was centrifuged at 2000 rpm and 4°C for 10 minutes to pellet cells. The supernatant was removed and the cell pellet was re-suspended in 2 ml sterile 0.9% saline. Total cell and viable cell counts were performed using a trypan blue exclusion dye assay in a hemocytometer under a light microscope. A cytospin slide was prepared from the resuspended BALF cells for cell differential determination. Slides were stained using DiffQuick stain kit (EMD Millipore) and 500 cells per slide were counted. Protein and lactate dehydrogenase (LDH) in BALF supernatant were determined using a Bradford protein assay (Bio-Rad, Hercules, CA) and LDH cytotoxicity assay (Cayman Chemical, San Diego, CA) following manufacturer protocols.

Deposition Modeling

Estimation of deposited dose of Gd_2O_3:Eu^{3+} NPs in adult rats was performed using two methods: (1) a general deposition equation: D = MCTF, where D is deposited dose, M is the minute volume (volume of air inhaled in one minute), C is concentration, T is exposure duration and F is the deposition fraction based on ICRP particle deposition modeling data,[25] and (2) the Multi-Path Particle Dosimetry Model (MPPD) v2.1 software (Applied Research Associates, Albuquerque, NM).[26] Input parameters for MPPD are listed in Table 2.

Statistics

Data are reported as mean ± standard error of the mean (SEM) unless otherwise stated. Statistical outliers were eliminated using the extreme deviate method (Graphpad, La Jolla, CA). Multivariate analysis of variance (MANOVA) was applied against age and exposure when appropriate. Multiple comparisons for factors containing more than two levels were performed using Fisher's Protected Least Significant Difference (PLSD) method. Pair-wise comparisons were performed individually using a one-way ANOVA followed by PLSD post hoc analysis. P values of < 0.05 were considered statistically significant. Statistics were calculated using STATISTICA 64 (Tulsa, OK).

Supplementary Material

Refer to Web version on PubMed Central for supplementary material.

Acknowledgments

The project described was supported by Award Number P42 ES004699 and U01 ES020127 from the National Institute of Environmental Health Sciences. The content is solely the responsibility of the authors and does not necessarily represent the views of the National Institute of Environmental Health Sciences or the National Institutes of Health. We thank the UC Davis Interdisciplinary Center for Inductively-Coupled Plasma Mass Spectrometry and both Peter Green and Joel Commisso for assistance with the ICP-MS samples and analysis. We thank the California National Primate Research Center Inhalation Exposure Core (P51 OD011107) and both Louise Olsen and Ashley Cooper for their assistance with gas testing. We thank the Cellular and Molecular Imaging Core (CAMI) for use of the microscopes including the TCS LSI confocal funded through grant # S10 RR026422. Sarah Carratt was supported by an NIEHS-funded predoctoral fellowship T32 ES007059. Support for core facilities by the UC Davis Environmental Health Sciences Core Center P30 ES023513 is gratefully acknowledged.

References

1. Lippmann M, Yeates DB, Albert RE. British journal of industrial medicine. 1980; 37:337–362. [PubMed: 7004477]
2. Xia T, Kovochich M, Liong M, Zink JI, Nel AE. ACS nano. 2008; 2:85–96. [PubMed: 19206551]
3. Choi HS, Ashitate Y, Lee JH, Kim SH, Matsui A, Insin N, Bawendi MG, Semmler-Behnke M, Frangioni JV, Tsuda A. Nature biotechnology. 2010; 28:1300–U1113.
4. Moller W, Felten K, Sommerer K, Scheuch G, Meyer G, Meyer P, Haussinger K, Kreyling WG. American journal of respiratory and critical care medicine. 2008; 177:426–432. [PubMed: 17932382]
5. Wiebert P, Sanchez-Crespo A, Falk R, Philipson K, Lundin A, Larsson S, Moller W, Kreyling WG, Svartengren M. Inhalation toxicology. 2006; 18:741–747. [PubMed: 16774863]
6. Cohen J, Deloid G, Pyrgiotakis G, Demokritou P. Nanotoxicology. 2013; 7:417–431. [PubMed: 22393878]
7. Kennedy IM. Proceedings of the Combustion Institute. 2007; 31:2757–2770.
8. Abid AD, Anderson DS, Das GK, Van Winkle LS, Kennedy IM. Particle and fibre toxicology. 2013; 10:1. [PubMed: 23305071]
9. US-EPA. [accessed 10/16/2012, 2012] Anaconda Mine. http://yosemite.epa.gov/r9/sfund/r9sfdocw.nsf/vwsoalphabetic/Anaconda+Mine?OpenDocument
10. Wells MA, Abid A, Kennedy IM, Barakat AI. Nanotoxicology. 2012; 6:837–846. [PubMed: 22149273]
11. Semmler-Behnke M, Kreyling WG, Schulz H, Takenaka S, Butler JP, Henry FS, Tsuda A. Proceedings of the National Academy of Sciences of the United States of America. 2012; 109:5092–5097. [PubMed: 22411799]
12. Tsuda A, Rogers RA, Hydon PE, Butler JP. Proceedings of the National Academy of Sciences of the United States of America. 2002; 99:10173–10178. [PubMed: 12119385]
13. Tsuda, A.; Henry, FS.; Butler, JP. Comprehensive Physiology. John Wiley & Sons, Inc; 2011.
14. Kreyling WG, Hirn S, Schleh C. Nature biotechnology. 2010; 28:1275–1276.
15. Oosterlee A, Drijver M, Lebret E, Brunekreef B. Occup Environ Med. 1996; 53:241–247. [PubMed: 8664961]
16. Chan JK, Charrier JG, Kodani SD, Vogel CF, Kado SY, Anderson DS, Anastasio C, Van Winkle LS. Particle and fibre toxicology. 2013; 10:34. [PubMed: 23902943]
17. Koenig JQ, Larson TV, Hanley QS, Rebolledo V, Dumler K, Checkoway H, Wang SZ, Lin DY, Pierson WE. Environmental Research. 1993; 63:26–38. [PubMed: 8404772]
18. Gauderman WJ, Gilliland GF, Vora H, Avol E, Stram D, McConnell R, Thomas D, Lurmann F, Margolis HG, Rappaport EB, Berhane K, Peters JM. American journal of respiratory and critical care medicine. 2002; 166:76–84. [PubMed: 12091175]
19. Sudheendra L, Das GK, Li C, Stark D, Cena J, Cherry S, Kennedy IM. Chemistry of materials : a publication of the American Chemical Society. 2014; 26:1881–1888. [PubMed: 24803724]
20. Das GK, Heng BC, Ng SC, White T, Loo JS, D'Silva L, Padmanabhan P, Bhakoo KK, Selvan ST, Tan TT. Langmuir : the ACS journal of surfaces and colloids. 2010; 26:8959–8965. [PubMed: 20148548]
21. Wang F, Banerjee D, Liu Y, Chen X, Liu X. The Analyst. 2010; 135:1839–1854. [PubMed: 20485777]
22. Zhang Y, Wei W, Das GK, Yang Tan TT. Journal of Photochemistry and Photobiology C: Photochemistry Reviews. 2014; 20:71–96.
23. Chatterjee DK, Yong Z. Nanomedicine. 2008; 3:73–82. [PubMed: 18393642]
24. Burri PH. Biology of the neonate. 2006; 89:313–322. [PubMed: 16770071]
25. ICRP. Annals of the ICRP. 1994; 24:79–98.
26. Anjilvel S, Asgharian B. Fundamental and Applied Toxicology. 1995; 28:41–50. [PubMed: 8566482]
27. Majeed S, Shivashankar SA. J Mater Chem C. 2014; 2:2965–2974.

28. Das GK, Tan TTY. J Phys Chem C. 2008; 112:11211–11217.
29. Goldys EM, Drozdowicz-Tomsia K, Jinjun S, Dosev D, Kennedy IM, Yatsunenko S, Godlewski M. J Am Chem Soc. 2006; 128:14498–14505. [PubMed: 17090033]
30. Raabe OG, Al-Bayati MA, Teague SV, Rasolt A. Annals of Occupational Hygiene. 1988; 32:53–63.
31. Oakes JM, Scadeng M, Breen E, Prisk GK, Darquenne C. Annals of biomedical engineering. 2013; 41:967–978. [PubMed: 23354670]
32. Sweeney TD, Brain JD, Leavitt SA, Godleski JJ. The American Journal of Pathology. 1987; 128:19–28. [PubMed: 3649192]
33. Oakes JM, Breen EC, Scadeng M, Tchantchou GS, Darquenne C. Journal of applied physiology. 2014; 116:1561–1568. [PubMed: 24790020]
34. Bennett WD, Scheuch G, Zeman KL, Brown JS, Kim C, Heyder J, Stahlhofen W. Journal of applied physiology. 1999; 86:168–173. [PubMed: 9887127]
35. Olvera HA, Perez D, Clague JW, Cheng YS, Li WW, Amaya MA, Burchiel SW, Berwick M, Pingitore NE. Pulmonary Medicine. 2012; 2012:736290. [PubMed: 22848818]
36. James AC, Stahlhofen W, Rudolf G, Köbrich R, Briant JK, Egan MJ, Nixon W, Birchall A. Annals of the ICRP. 1994; 24:231–299.
37. Garcia GJM, Kimbell JS. Inhalation toxicology. 2009; 21:1165–1175. [PubMed: 19831956]
38. Weiler E, Farbman AI. The Journal of neuroscience : the official journal of the Society for Neuroscience. 1997; 17:3610–3622. [PubMed: 9133384]
39. Massaro GD, Massaro D. Annual Review of Physiology. 1996; 58:73–92.
40. Blanco LN, Massaro GD, Massaro D. Alveolar dimensions and number: developmental and hormonal regulation. 1989
41. Burri PH. The Anatomical Record. 1974; 180:77–98. [PubMed: 4416419]
42. Tschanz SA, Salm LA, Roth-Kleiner M, Barre SF, Burri PH, Schittny JC. Journal of applied physiology. 2014; 117:89–95. [PubMed: 24764134]
43. Londahl J, Moller W, Pagels JH, Kreyling WG, Swietlicki E, Schmid O. Journal of aerosol medicine and pulmonary drug delivery. 2014; 27:229–254. [PubMed: 24151837]
44. Miller FJ, Asgharian B, Schroeter JD, Price O, Corley RA, Einstein DR, Jacob RE, Cox TC, Kabilan S, Bentley T. Inhalation toxicology. 2014; 26:524–544. [PubMed: 25055841]
45. Ji JH, Yu IJ. Toxicology Research. 2012
46. Chan JKW, Fanucchi MV, Anderson DS, Abid AD, Wallis CD, Dickinson DA, Kumfer BM, Kennedy IM, Wexler AS, Van Winkle LS. Toxicological Sciences. 2011; 124:472–486. [PubMed: 21914721]
47. Terraschke H, Wickleder C. Chem Rev. 2015; 115:11352–11378. [PubMed: 26395168]
48. Dosev D, Guo B, Kennedy IM. Journal of Aerosol Science. 2006; 37:402–412.
49. Raabe OG, Bennick JE, Light ME, Hobbs CH, Thomas RL, Tillery MI. Toxicology and Applied Pharmacology. 1973; 26:264–273. [PubMed: 4751105]
50. Wilson HH, Chauhan J, Kerry PJ, Evans JG. J Immunol Methods. 2001; 247:187–190. [PubMed: 11150549]
51. Hammond TG, Mobbs M. J Appl Toxicol. 1984; 4:219–221. [PubMed: 6208233]
52. Sutherland KM, Edwards PC, Combs TJ, Van Winkle LS. Sex differences in the development of airway epithelial tolerance to naphthalene. 2012

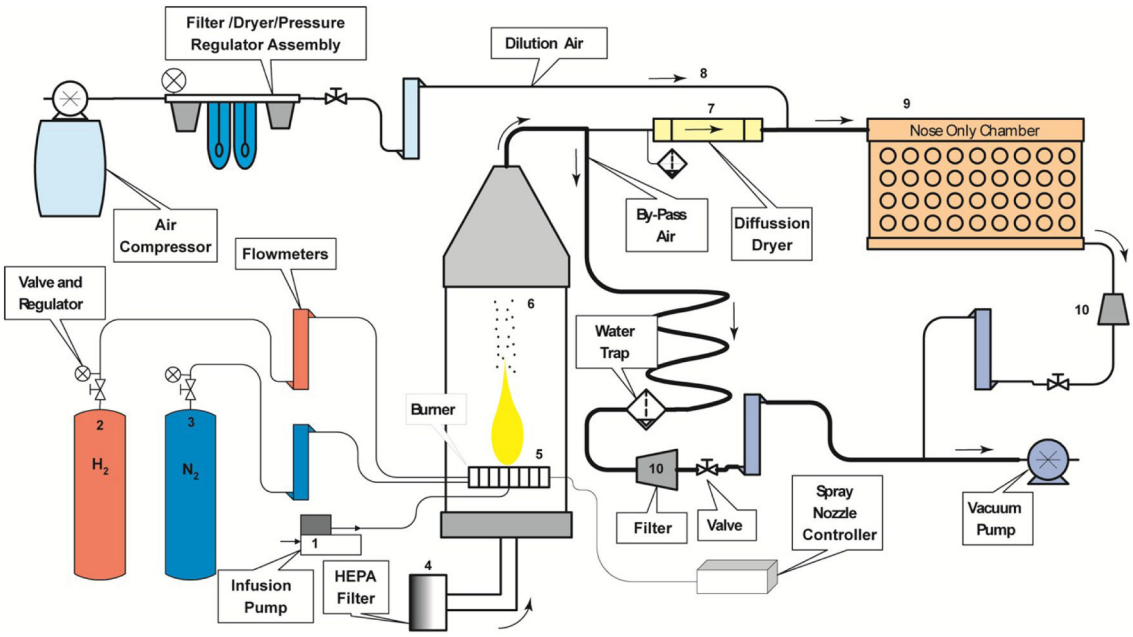

Figure 1. Schematic of the nanoparticle generation and exposure system

Europium and gadolinium salts dissolved in water constitute the precursor solution (infusion pump, 1). Hydrogen gas (2) was used for the burner fuel and nitrogen gas (3) as the carrier for the precursor droplets. Room air is HEPA filtered (4) before being drawn into the burner chamber. The infusion pump delivers the precursor to the burner assembly (5) were the precursor is atomized into droplets using an ultrasonic atomizer. Particles formed by pyrolysis (6) are drawn from the burner chamber were a fraction of generated particles are passed through a diffusion dryer (7) to remove moisture generated by the combustion of hydrogen. Dried and filtered air was mixed with the particle stream to produce the desired dilution. The diluted particle stream was then directed to the nose only exposure chamber (9) were rats were exposed nose only for one hour. Excess particles from the exposure chamber and the by-pass airflow were collected on filters. Arrows indicate direction of air/particle flow.

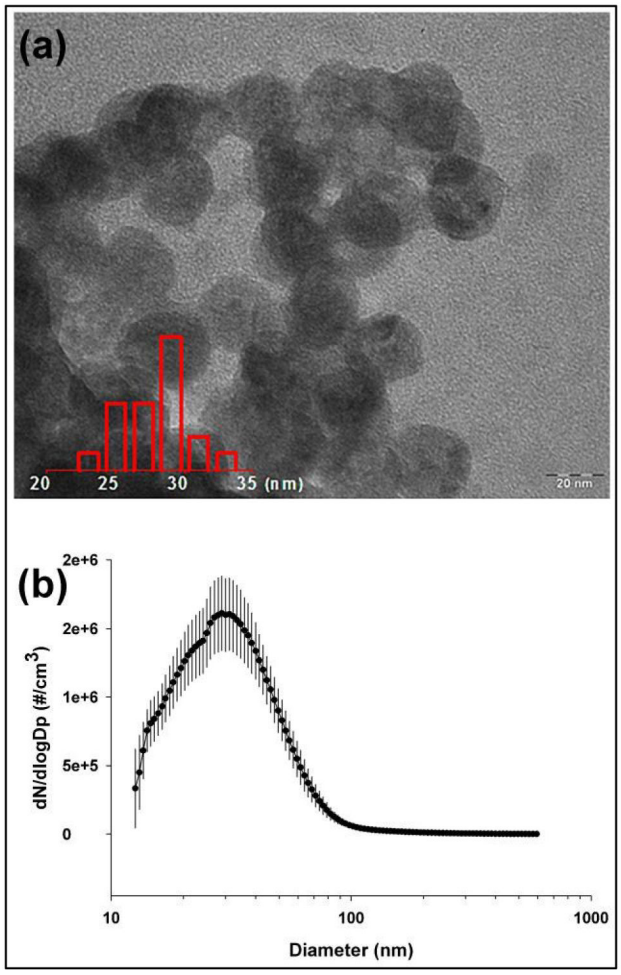

Figure 2. Size distribution on Gd_2O_3:Eu^{3+} NPs

(a) Typical TEM image of the flame synthesized Gd_2O_3:Eu^{3+} NPs. Inset shows the size distribution obtained from more than 100 nanoparticles by TEM. (b) Aerodynamic size distribution of the particles obtained from SMPS measurements. Error bars represent standard deviation from the mean. Scale bar = 20 nm.

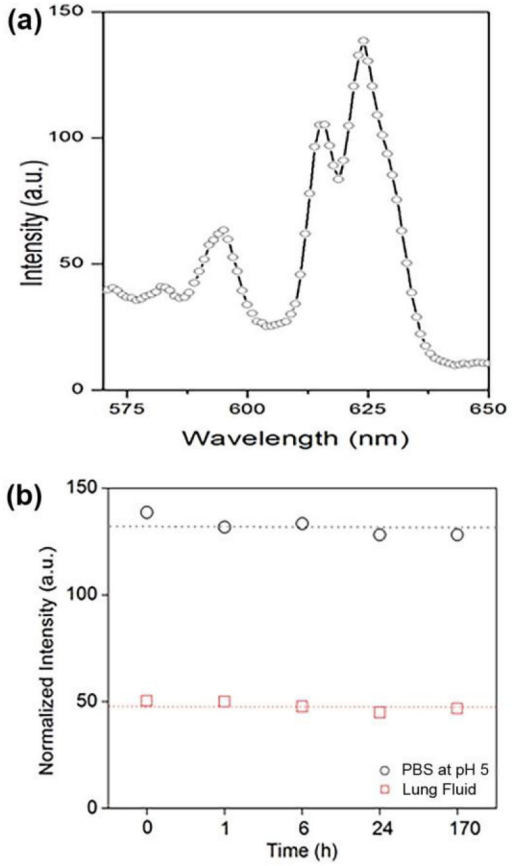

Figure 3. Stability of $Gd_2O_3:Eu^{3+}$ NPs over time

(a) Photoluminescence (PL) spectrum of $Gd_2O_3:Eu^{3+}$ NPs at 254 nm excitation, (b) Normalized PL intensity based on area under the curve of the nanoparticles' dispersion in PBS buffer (black circles) and lung lavage fluid (red squares) from 0 to 170 h of incubation showing no decrease of luminescence over time in either PBS or lung lavage fluid.

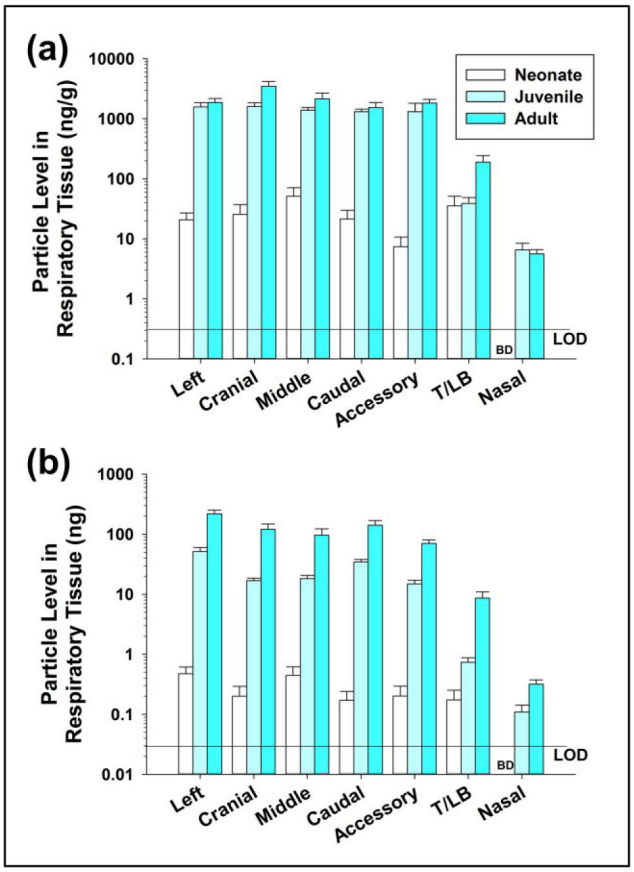

Figure 4. Deposition of nanoparticles in the lung and extrapulmonary (lobar bronchus and trachea) airways at the end of 1 h nose only exposure

(a) Nanograms of total Gd_2O_3:Eu^{3+} NPs deposited in each region examined. This indicates the mass of deposited nanoparticle without regard to the size of that region or size of the animal. (b) Nanoparticles per gram of dry lung tissue of each respiratory region. This measure takes into account the increase tissue mass of different regions and the size difference between animals of different ages. LOD: Level of Detection, BLD: Below Level of Detection. (n=5)

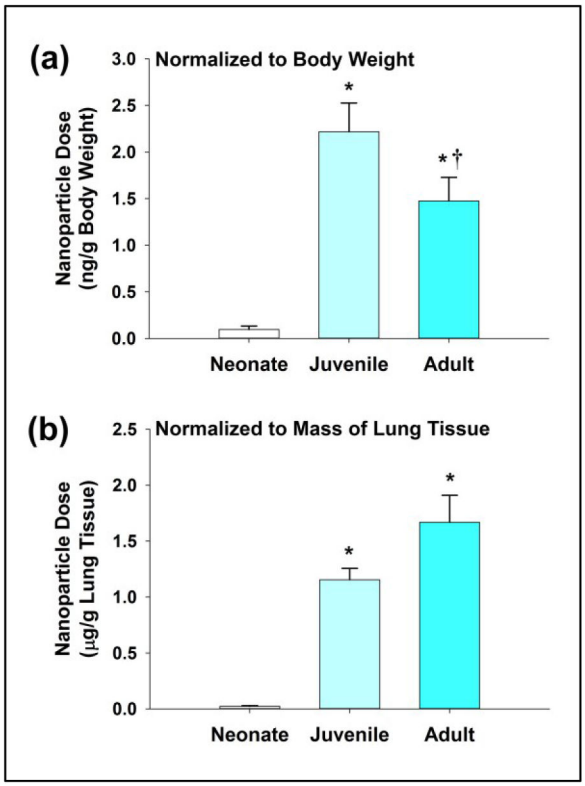

Figure 5. Delivered dose of nanoparticles to three ages of rats

For this comparison, we summed the deposited mass of nanoparticles in the entire respiratory tract for each animal and divided by the animal's body weight at the time of necropsy (a) Dose of Gd_2O_3:Eu^{3+} NPs **per gram of body weight rats** received during a one hour nose only inhalation exposure to 380 μg/m^3 of particles. The mass of deposited particles was deterined by ICP-MS and body weight was measured at completion of exposure. (b) The dose of Gd_2O_3:Eu^{3+} NPs deposited in the whole lung **in proportion to the mass of lung tissue**. * significantly different than neonatal animals, † significantly different than juvenile animals. ($p<0.05$, n=5)

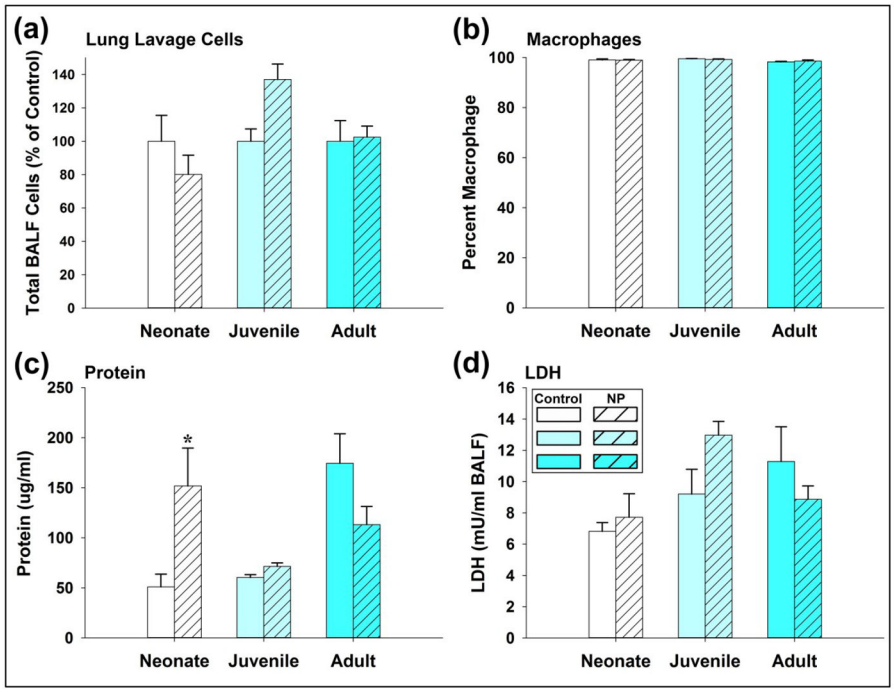

Figure 6. Indicators of inflammation and cytotoxicity

(A) When normalized for lung lavage volume, there were no differences between exposed and control animals for each of the age groups. However, the total cells in adult rats were lower than the total cells in both juvenile and neonate rats. (B) Percent of macrophages was not different between groups, with 98 to 99% of recovered cells being macrophages. (C) There was significantly higher protein level in exposed neonatal rats suggests capillary leakage. There was no difference between controls and exposed for adult and juvenile rats. (D) LDH activity in BALF is an indicator of cell permeability. There was no significant difference between the exposed and control animals at any of the ages, indicating lack of cellular damage. * significantly differenrent than control group of same age ($p<0.05$, $n=5$)

Figure 7. Stability of $Gd_2O_3:Eu^{3+}$ NPs in a macrophage in the alveoli of the lung

Fluorescent image of alveolar macrophage with internalized $Gd_2O_3:Eu^{3+}$ NPs. Image taken from whole mount tissue sample from an adult rat 24 h post exposure using fluorescent microscope and water dipping lens. Excitation λ =340–380 nm. Bar ~10 μm.

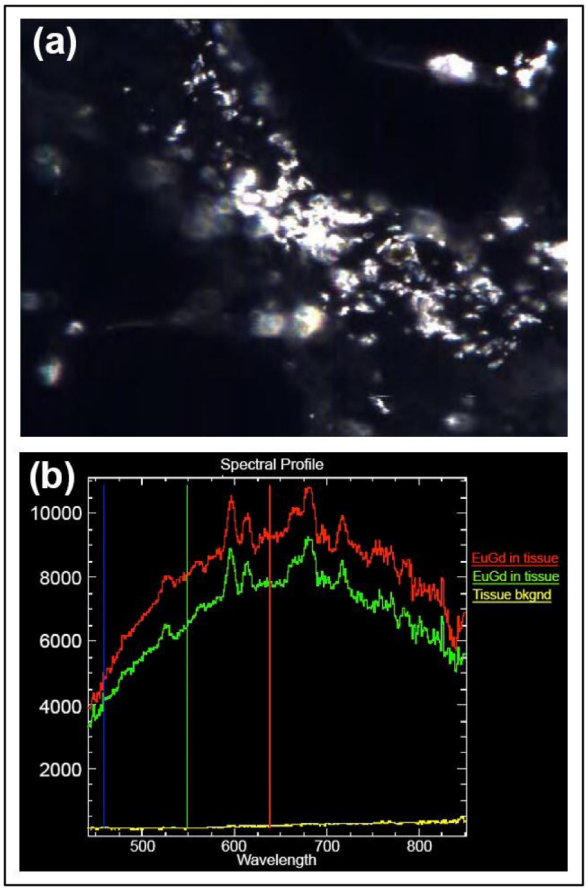

Figure 8. Cytoviva enhanced dark field imaging and spectral analysis

(a) Image of 4 μm lung tissue using enhanced dark field imaging following exposure to Gd_2O_3:Eu^{3+} NPs. Bright sections of image indicate deposition of particles on the alveolar epithelium. (b) Spectral profile of Gd_2O_3:Eu^{3+} NPs in lung tissue. Samples are from adult rat with 24 h post exposure.

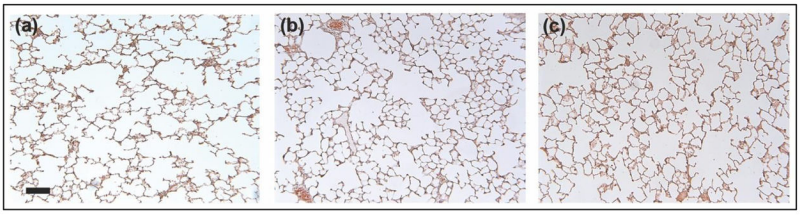

Figure 9.

Representative H&E stained lung tissue illustrating developmental differences in the gas exchange region of the lung in (a) 1 week old neonate, (b) 3 weeks old juvenile, and 12 weeks old adult rats. Scale Bar = 100 μm.

Table 1

Characteristics of the nanoparticle generation and exposure system. Measurements listed were taken from a port of the nose only exposure system except when noted as coming from the burner-housing outlet (pre-dilution).

Parameters	Values
Geometric Mean Mobility Diameter	31.1nm σ_g 1.6
Particle Number Concentration	$7.4\times10^5/cm^3$
Mass Concentration	380 $\mu g/m^3$
CO	< 0.5 ppm (pre-dilution)
NO	0.45 ppm (pre-dilution)
NO_2	0.45 ppm (pre-dilution)
VOC	0.2 ppm (pre-dilution)
Temperature	< 1°C of ambient
Relative Humidity	30 – 35% during animal exposures (6% min.)

Table 2

Multi Path Particle Dosimetry (MPPD) model input parameters and results for the Gd_2O_3:Eu^{3+} nanoparticles exposure to adult rats.

Input Parameters	
FRC Volume (ml) [1]	4.0
Head Volume (ml) [1]	0.42
Density	7.46
Diameter (CMD)(nm)	29.6[3]
Geometric SD (σ_g)	1.6
Concentration (μg/m^3)	380
Breathing Freq[1] (min^{-1})	102
Tidal Volume[1] (ml)	2.1
Inspiratory Fraction[1]	0.5
Pause Fraction[1]	0
Breathing Scenario	Nasal
Clearance Rate[2] (day^{-1})	0.00515
Output (Results)	
Deposition Fraction Alveolar Region	0.2490
Deposition Fraction Conducting Airways	0.0623
Deposited Fraction Head	0.116
Total Deposited Fraction	0.428
Mass: Pulmonary (μg)	1.228
Mass: Tracheal/Bronch (μg)	0.2146

[1] Default value from the MPPD software;

[2] Ji and Yu, 2012 Toxicology Research;

[3] SMPS data